*DOI:*
10.1016/j.jmbbm.2019.03.018

*Document Version*
Peer reviewed version

# Effect of cell sample size in atomic force microscopy nanoindentation

Stefania Marcotti [a, b, c*] (stefania.marcotti@kcl.ac.uk),
Gwendolen C Reilly [a, d] (g.reilly@sheffield.ac.uk),
Damien Lacroix [a, b] (d.lacroix@sheffield.ac.uk)

a. Insigneo Institute for in silico Medicine
University of Sheffield
Mappin Street
Sheffield S1 3JD, UK
b. Department of Mechanical Engineering
University of Sheffield
Western Bank
Sheffield S10 2TN, UK
c. Randall Centre for Cell and Molecular Biophysics
King's College London
Guy's Campus
London SE1 1UL, UK
d. Department of Materials Science and Engineering
University of Sheffield
Western Bank
Sheffield S10 2TN, UK

* Corresponding author

## Abstract

Single-cell technologies are powerful tools to evaluate cell characteristics. In particular, Atomic Force Microscopy (AFM) nanoindentation experiments have been widely used to study single cell mechanical properties. One important aspect related to single cell techniques is the need for sufficient statistical power to obtain reliable results. This aspect is often overlooked in AFM experiments were sample sizes are arbitrarily set.

The aim of the present work was to propose a tool for sample size estimation in the context of AFM nanoindentation experiments of single cell. To this aim, a retrospective approach was used by acquiring a large dataset of experimental measurements on four bone cell types and by building saturation curves for increasing sample sizes with a bootstrap resampling method.

It was observed that the coefficient of variation ($CV_{\%}$) decayed with a function of the form $y = ax^b$ with similar parameters for all samples tested and that sample sizes of 21 and 83 cells were needed for the specific cells and protocol employed if setting a maximum threshold on $CV_{\%}$ of 10% or 5%, respectively. The developed tool is made available as an open-source repository and guidelines are provided for its use for AFM nanoindentation experimental design.

Keywords: sample size; atomic force microscopy; nanoindentation; bone cells.

## 1. Introduction

Single cell analysis technologies have recently enabled unprecedented access to specific biological features, with higher resolution than that provided with bulk analyses (Tsioris et al., 2014). Single cells in a population show variable behaviours and characteristics: this heterogeneity has stochastic as well as deterministic sources and historically has often been overlooked when focusing on common mechanisms between cells (Pelkmans, 2012). Most information collected on cell processes was obtained averaging the characteristics of a cell population and generalising them to all cells (Chen et al., 2016). However, when the same characteristics were studied at the single cell level different patterns might have emerged, highlighting the fact that cell-to-cell heterogeneity often dictates relevant functions for homeostasis.

Single cell technologies have been mostly used to measure nucleic acids, proteins, lipids and metabolites content (Chen et al., 2016) in the context of cancer biology and immune system response (Love, 2010; Navin, 2014; Papalexi and Satija, 2017; Tsioris et al., 2014; Wang et al., 2017). However, similar approaches can be employed to quantify characteristics of single cells at a higher dimensional scale, such as whole cell mechanical properties. Single cell mechanical properties have been tested with various methods, such as micro-aspiration, optical tweezers and atomic force microscopy (AFM) (Costa, 2004). Recently, the latter technique has been largely employed due to its ability to perform controlled nanoindentation of biological samples (Kuznetsova et al., 2007; Müller and Dufrêne, 2011).

In the case of single cell AFM nanoindentation, different factors have been proposed to contribute to population heterogeneity. Cell cycle stage, differentiation status (Crisan and Dzierzak, 2016; Krieger and Simons, 2015; Satir, 2016), migration capability and adhesion to the substrate (Wills et al., 2017) all have a direct impact on the cell cytoskeleton and therefore on the cell mechanical properties. Moreover, the experimental set-up, the testing and culture conditions, and the post-processing of data might all introduce technical variability (Costa, 2004; Kuznetsova et al., 2007; Lekka, 2016; Luo et al., 2016).

A factor that should be taken into account when designing single-cell experiments relates to the statistical power of the analysis (Chen et al., 2016; Wagner et al., 2016). Optimal trade-

offs in terms of the number of cells to be tested and the number of reads to be performed per cell should be set accordingly to the experiment and research question. A correct estimate of the required sample size relies on the diversity of the underlying population, the sensitivity required for the measure and the technical variability of the measure. Often an arbitrary number of cells is tested causing unreliability in the obtained results (Chen et al., 2016; Krzywinski and Altman, 2013).

Different AFM experimental protocols and data analysis techniques have been used to test single cell mechanical properties leading to difficulties when comparing different results. In particular, the number of cells tested and the number of measurement repeats per cells were found to be highly variable (e.g. Bacabac et al., 2008; Bongiorno et al., 2014; Docheva et al., 2008; Muthukumaran et al., 2012; Sugawara et al., 2008; Takai et al., 2005) and to the best of our knowledge, no sample size analysis was performed in the context of AFM nanoindentation experiments.

The objective of the present work was therefore to propose a tool for sample size analysis of AFM nanoindentation experiments. To this aim, a retrospective estimation approach was chosen, i.e. a great number of experimental datasets were obtained and the cumulative average stiffness was plotted as a function of the cumulative number of single cells resulting in a saturation curve (Chen et al., 2016). This tool was tested by using large datasets of AFM nanoindentation measurements, acquired and analysed *ad hoc* for this study. The impact of repeated measurements per cell was evaluated. Guidelines to use this tool for future experimental designs are proposed.

## 2. Materials and Methods

### 2.1 Cells

Three cell lines representing four bone cell types were used for this study, namely MC3T3 pre-osteoblast (Kodama et al., 1981), IDG-SW3 osteoblast and osteocyte (Woo et al., 2011), and MLO-A5 pre-osteocyte cells (Kato et al., 2001). MLO-A5 cells were kindly donated by Prof. Lynda Bonewald (University of Missouri, Kansas City, MO, USA). IDG-SW3 cells can represent separate stages of differentiation from late osteoblast to late osteocyte thanks to a temperature sensitive mutant protein controlled by interferon-γ (INF-γ) (Wittkowske et al., 2016; Woo et al., 2011). The undifferentiated osteoblast-like and differentiated osteocyte-like stages can be optically distinguished thanks to green fluorescent protein (GFP) tagged dentin matrix acidic phosphoprotein 1 (Dmp1), i.e. cells express green fluorescence when differentiated.

MC3T3 and MLO-A5 cells were cultured at 37°C in Minimum Essential Alpha Eagle medium (αMEM, Lonza Group Ltd., Basel, Switzerland) supplemented with 10% foetal bovine serum (FBS, Labtech International Ltd., Heathfield, UK), 100 units/ml penicillin, 100 µg/ml streptomycin and 2 mM glutamine (PSG, Sigma-Aldrich Company Ltd., Gillingham, UK). Osteoblast-like IDG-SW3 cells were cultured at 33°C in αMEM supplemented with nucleosides and 2 mM UltraGlutamine I, 10% FBS, 50 units/ml INF-γ (Fisher Scientific) and a solution of 100 units/ml penicillin and 100 µg/ml streptomycin (PS, Sigma). To induce osteogenic differentiation, IDG-SW3 cells were cultured at 37°C in differentiation medium, constituted of αMEM supplemented with nucleosides and 2 mM UltraGlutamine I, 10% FBS, 1% PS, 5mM β-glycerophosphate (Sigma) and 50 µg/ml L-ascorbic acid 2-phosphatesesquimagnesium salt hydrate (ascorbic acid, Sigma). Cells were monitored under fluorescent microscopy for the onset of GFP signal, representing the marker for differentiation. After 10-12 days in culture in differentiation medium, IDG-SW3 cells expressed a detectable GFP signal and were classified as osteocyte-like.

Prior to AFM experiments, cells were seeded onto tissue culture treated plastic dishes (D = 10 mm) at low seeding density to obtain spatially separated cells during testing. For osteocyte-like IDG-SW3 cells, each cell GFP signal was verified prior to testing as it was observed that the GFP signal would fade after some time in culture at low density.

## 2.2 AFM cantilever preparation

Spherical tipped cantilevers were produced following a similar protocol as described elsewhere (Li et al., 2016). Tip-less cantilevers (Windsor Scientific Ltd, Slough, UK) with a nominal spring constant of 0.2 N/m were customised by glueing a silica bead (D = 6±0.2 µm, Bangs Laboratories Inc., Fishers, IN) at the tip extremity. The cantilever spring constant calibration was performed in liquid prior to bead attachment with the AFM built-in software by thermal noise method. The average spring constant measured by thermal calibration prior to bead attachment was 0.26 N/m.

## 2.3 AFM set-up

A NanoWizard 3 AFM (JPK Instruments AG, Berlin, Germany) coupled to an Eclipse Ti-S optical inverted microscope (Nikon UK Ltd., Kingston Upon Thames, UK) was used for all the experiments. The cells were washed in phosphate buffer solution (PBS, Sigma) and fresh medium was added. Samples were positioned on the heated sample holder to allow for testing at 37°C (33°C for osteoblast-like IDG-SW3 cells). The cantilever sensitivity was calibrated on the bare tissue culture plate before each experiment.

The cantilever was centred over the cell nucleus and a grid of five points spaced 3 µm within each other was set (Takai et al., 2005). Force spectroscopy measurements were obtained on the 5-point grid three times to collect a total of 15 data on the nuclear region. The same procedure was performed at the cell periphery. The relative set point and the approach velocity were set to 10 nN and 4 µm/s respectively. A total of 178 MC3T3 cells were indented over 3 separate experiments, 192 osteoblast-like IDG-SW3 cells were indented over 4 separate experiments (nuclear region only), 180 MLO-A5 cells were indented over 3 separate experiments, and 160 osteocyte-like IDG-SW3 cells were indented over 4 separate experiments.

## 2.4 AFM post-processing

The obtained data files were exported as text files from the JPK Data Processing software. All the subsequent post-processing was performed in MATLAB (The MathWorks, Natick, MA) with custom-written semi-automated algorithms to allow for careful tailoring of the analysis steps. Each force spectroscopy extend curve was analysed separately to fit the contact point and to obtain the effective modulus as a measure of cell stiffness. The effective modulus of a given cell was obtained by averaging the values obtained for each indentation on that cell hypothesising spatial homogeneity over the tested region (nucleus or periphery), thanks to the global information obtained by using spherical probes which reduced the impact of local inhomogeneity at the nanoscale (Puricelli et al., 2015).

The ratio of variance method proposed in (Gavara, 2016) was used to determine the contact point, i.e. the point in the force spectroscopy curve at which the probe first comes into contact with the cell. Each force spectroscopy curve was visually checked to verify the algorithm correct functioning: curves displaying no baseline were discarded. Pre-processed data are made available on Figshare at the following DOI: 10.15131/shef.data.5632777.

The cell effective modulus $E^*$ was obtained by Hertz model fitting on the extend force spectroscopy curve. The Hertz model formulation for a spherical indenter over a half space (Hertz, 1881; Kuznetsova et al., 2007) was used, with $F$ force on the indenter, $i$ indentation depth and $R$ radius of the indenter (Eq. 1, Figure 1):

$$F(i) = \frac{16}{9} E^* R^{\frac{1}{2}} i^{\frac{3}{2}} .\#(1)$$

The data were fitted up to an equal indentation depth for all the curves in a sample, which was set by considering the last indentation value for which more than 90% of force spectroscopy data were available. This varied between 200-800 nm depending on cell type and testing location. The extreme case of an indentation of 800 nm was found for the MLO-A5 cells tested on the nucleus region and was further investigated by measuring the average cell thickness of adherent MLO-A5 cells. This was tested with QI™ AFM mode on a 10-cell sample during preliminary studies under similar culture conditions and resulted equal to 2.46 (0.30) μm. Therefore, a maximum indentation of 800 nm could affect ~33% of the cell thickness. Previous work on Chinese hamster ovary cells showed that indentations of up to 50% of the cell thickness did not display a substrate contribution (Zhao et al., 2006), and the analysis was therefore performed by using this maximum indentation value. The coefficient of determination ($R^2$) was obtained as an indicator of the goodness of fit of the Hertz model to the data.

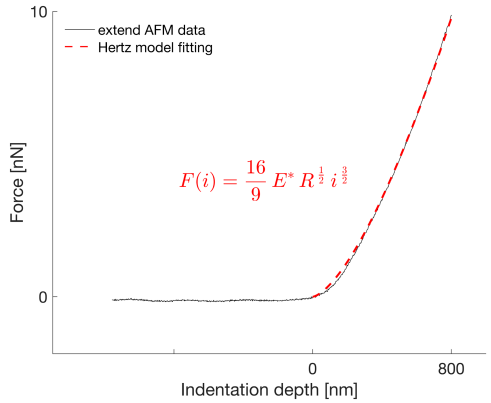


*Figure 1 – **Force spectroscopy fitting.** Example (MLO-A5 cell, nucleus) of force spectroscopy curve fitting to obtain the effective modulus E*, with the pre-processed extend data represented in black and the Hertz model fitting in red (dashed line). The equation of the Hertz model for a spherical indenter over a half space is reported.*

## 2.5 Sample size analysis

A retrospective estimation approach was employed to quantify the number of cells to be tested in order to achieve a reliable measurement of the population average stiffness. To this aim, an algorithm was designed to compute the convergence effective modulus for each sample size, as schematised in Figure 2. For each sample size N up to the number of cells tested in each sample, N cells are randomly chosen (draw D) from the list with a bootstrap approach (with replacement) and their instant average modulus $E_D$ is calculated. The average modulus $E_D$ for the D-th draw is used to calculate a cumulative modulus by using all the previous draws and computing a cumulative average $\mu_N$ and standard deviation $\sigma_N$. Draws are continued until convergence of $\mu_N$ and $\sigma_N$ is reached. The convergence threshold is set to the percentage error of $\mu_N$ and $\sigma_N$ for subsequent draws being lower than 1% for 50 subsequent draws.

By applying this algorithm to the data, the convergence effective modulus average $E_N$ and standard deviation $\sigma E_N$ for each sample size were computed. These values were used to calculate the coefficient of variation ($CV_{\%}$ = 100 * $\sigma E_N / E_N$) used to plot saturation curves.

A similar procedure was applied to two subsets of data for one cell type in order to evaluate how the saturation curve would change if fewer measurements were taken for each cell. The first subset consisted of three measurements per cell (central grid point, tested in three

subsequent series); the second subset was made of one measurement per cell (central grid point, first series).

The sample size calculator and the coding to obtain the effective modulus from the AFM force-spectroscopy data are available at the following GitHub repository: INSIGNEO/ AFM_Youngs_modulus_fit.

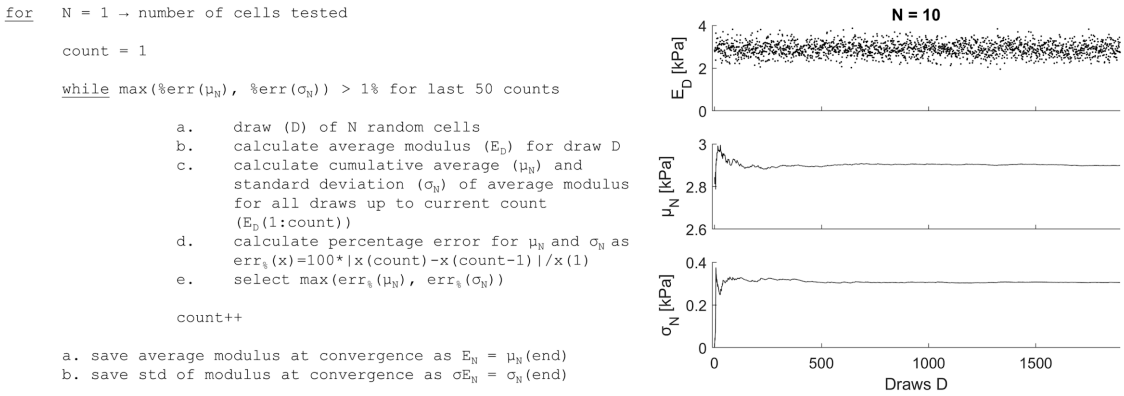


*Figure 2 – **Effective modulus at convergence, schematic of the algorithm.** A representation of the algorithm to find the effective modulus at convergence for each sample size is shown on the left. Example plots for N=10 are shown on the right, for the instant average modulus $E_D$, the cumulative modulus average $\mu_N$ and standard deviation $\sigma_N$ for subsequent draws. In this example, 8193 draws were necessary to reach convergence to a cumulative modulus of 2.90 (0.31) kPa.*

# 3. Results

## 3.1 Effective modulus distributions

A total of 2033 and 2453 indentations across 175 and 177 different MC3T3 cells were analysed for the nucleus and periphery, respectively; a total of 1778 indentations across 190 different IDG-SW3 osteoblast-like cells were analysed for the nucleus; a total of 2137 and 2556 indentations across 168 and 180 different MLO-A5 cells were analysed for the nucleus and periphery, respectively; a total of 1214 and 645 indentations across 144 and 79 different IDG-SW3 osteocyte-like cells were analysed for the nucleus and periphery, respectively. The Hertz model fitting quality was generally high ($R^2$ = 0.96 (0.05)).

By hypothesising each cell to have spatially homogeneous stiffness properties described by the average value of all measurements, the average and dispersion values for the cell population were calculated by using the average value from single cells (not normal distribution of cell effective modulus values across the population). Histograms of the single cell average effective modulus values normalised for the total number of cells were calculated for each cell line, for the nucleus and periphery (Figure 3). Average and dispersion values are reported in Table 1.

The periphery effective modulus values were larger than the nuclear ones for all cell lines. MC3T3 and MLO-A5 cells showed lower and less disperse stiffness in both the nucleus and peripheral regions. In contrast, the osteoblast- and osteocyte-like IDG-SW3 cells showed wide dispersion ranges and higher values.

Each cell was repeatedly indented 15 times in five 3μμ-spaced locations over the nucleus and 15 times in five 3μμ-spaced locations over the periphery. This could result in a time-dependent viscoelastic response of the cell which could potentially start to rearrange its actin cytoskeleton (Lekka, 2016). To investigate the occurrence of this phenomenon, the effective modulus distributions for different indenting locations within the test grid (i.e. the measurements obtained for the five points of each grid) and for different series of

indentations (i.e. the measurements obtained for the three indentation series) were compared and no difference was found (Kruskal-Wallis non-parametric test, significance set at $p < .01$, data not shown), also justifying the hypothesis of spatial homogeneity within tested regions. It should be noted that these results are valid for the specific loading rate used in this protocol, as higher loading rates could lead to higher measured effective moduli (Zhao et al., 2006).

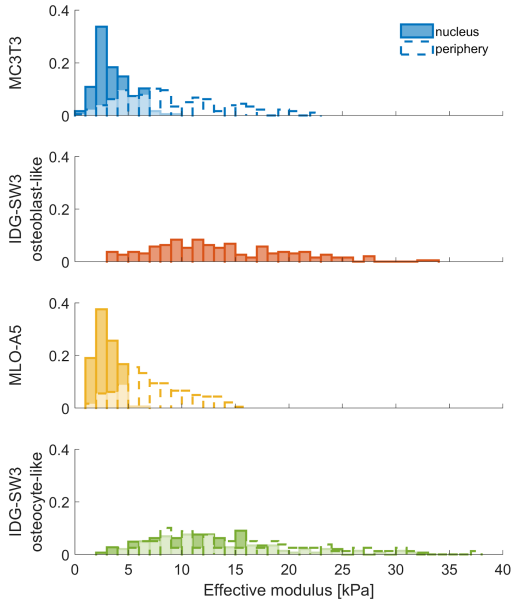


*Figure 3 – **Effective moduli for bone cells.** Histograms of single cell average effective moduli for all tested cell lines (MC3T3 cells in blue, IDG-SW3 osteoblast-like cells in orange, MLO-A5 cells in yellow and IDG-SW3 osteocyte-like cells in green), normalised for the total number of cells. Histograms for the nuclear area have shaded fill, histograms for the peripheral area have no fill.*

*Table 1 – **Effective moduli for bone cells.** Median (inter-quartile range) of the effective moduli [kPa] for all tested cells on the nuclear and peripheral regions*

| Cell type | Effective modulus [kPa] | |
|---|---|---|
| | Nucleus | Periphery |
| MC3T3 | 3.19 (2.16) | 8.21 (6.88) |
| IDG-SW3 osteoblast-like | 12.33 (8.91) | - |
| MLO-A5 | 2.81 (1.50) | 6.93 (4.66) |
| IDG-SW3 osteocyte-like | 11.87 (7.24) | 14.33 (11.90) |

## 3.2 Sample size analysis: how many cells?

All the calculations reported so far were performed on the data relative to all available cells. However, smaller samples might be sufficient to reliably estimate the mechanical characteristics of each cell type. The algorithm described for the retrospective power estimate was therefore applied to all samples, divided by cell type and region of testing (nucleus, periphery). This allowed the building of saturation curves for the coefficient of variation ($CV_{\%}$) for increasing sample sizes.

An example for the MLO-A5 cells tested on the nuclear region is shown in Figure 4. The convergence effective modulus $E_N$ tends to a constant value and the standard deviation decreases for increasing sample sizes N. This is mirrored in the $CV_{\%}$, which decays toward zero for increasing sample sizes. All the tested cell types for both the nuclear and peripheral regions showed similar trends (Figure 5, left and central panels), therefore a common fitting was performed with a non-linear least squares method with an equation of the form $y = ax^b$ (Figure 5, right panel).

Good fitting quality was achieved ($R^2 = 0.96$), with the following parameters (95% confidence bounds): a = 46.0 (45.5, 46.6) and b = -0.50 (-0.51, -0.50). It was possible to calculate the number of cells needed to achieve a given maximum $CV_{\%}$ by using the fitted curve (Figure 5, right panel): 21 cells would suffice if setting a threshold for a maximum $CV_{\%}$ of 10%, 83 cells for 5%.

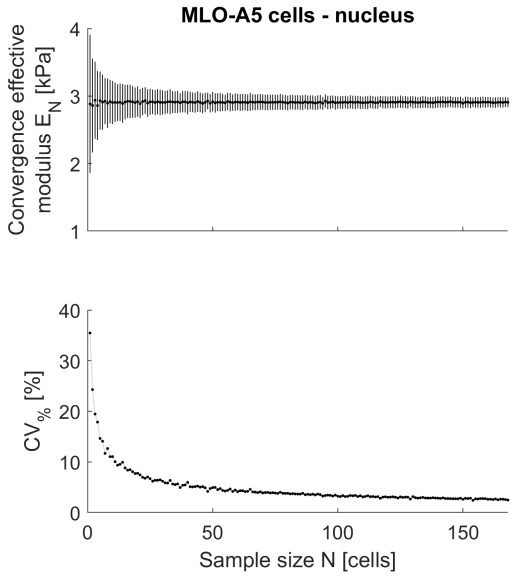


*Figure 4 – **Evaluation of sample size, effective modulus at convergence.** Top panel: error bar plot of the convergence effective modulus $E_N$ for increasing sample size N. Bottom panel: coefficient of variation ($CV_{\%}$) saturation curve for increasing samples sizes. Both plots are for the MLO-A5 cells tested on the nuclear region.*

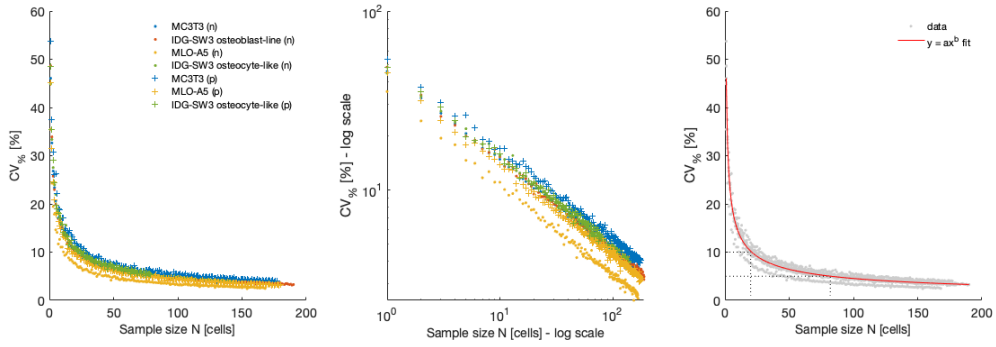


*Figure 5 – **Evaluation of sample size, analytical fitting.** Left panel: the CV% saturation curve for increasing sample sizes N are shown for all cell types and regions tested (MC3T3 cells in blue, IDG-SW3 osteoblast-like cells in orange, MLO-A5 cells in yellow and IDG-SW3 osteocyte-like cells in green; dot markers represent the nucleus (n), cross markers the periphery (p)). Central panel: the same data shown in the left panel is displayed in log-log scale. Right panel: a common fitting with a curve of the form $y = ax^b$ (red line) was performed on the data (grey dots). The dotted lines show how many cells are needed if setting a threshold of 10% (21 cells) or 5% (83 cells) on the $CV_{\%}$.*

### 3.3 Sample size analysis: how many measurements per cell?

The cell type/region combination with narrower effective modulus distribution (i.e. MLO-A5 cells in the nuclear region, Figure 3) was used for this analysis. The distributions of effective modulus for each cell obtained by using only one measurement (1 point tested once) or by averaging 3 (1 point tested thrice) or 15 measurements (5-point grid tested thrice) were compared (Figure 6, left panel). The values for the average and dispersion for each distribution are reported in Table 2. The distribution dispersion decreased with increasing number of measurements averaged per cell.

The data from the different distributions were then used to calculate the required sample size. The coefficient of variation $CV_{\%}$ plotted against the sample size N can be found in Figure 6 (right panel). By averaging higher number of measurements per cell it was possible to obtain similar $CV_{\%}$ with lower samples sizes.

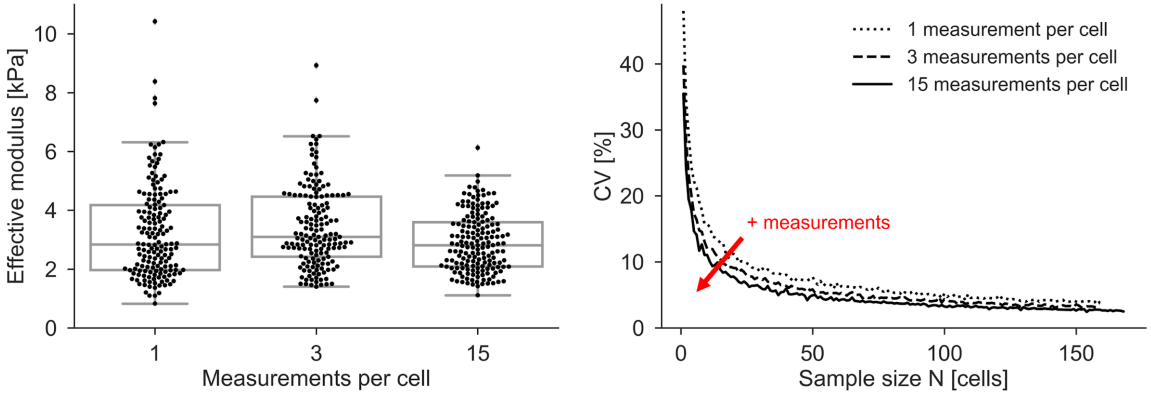


*Figure 6 – **Evaluation of sample size, number of measurements per cell.** Left panel: Swam plot of effective modulus distributions for increasing number of measurements averaged per cell. The plot refers to the MLO-A5 cell type and the nuclear region. The distribution spread decreased with increasing number of measurements per cell. Right panel: coefficient of variation $CV_{\%}$ plotted against the sample size N for increasing number of measurements averaged per cell. Similar $CV_{\%}$ were achieved with smaller sample sizes if increasing the number of measurements per cell (red arrow).*

*Table 2 – **Effective modulus for increasing number of measurements per cell.** Median (inter-quartile range) of the effective moduli [kPa] for the MLO-A5 cells tested in the nuclear region obtained by using 1, 3 or 15 measurements per cells*

| Measurements per cell | Effective modulus [kPa] |
|---|---|
| 1 | 2.84 (2.22) |
| 3 | 3.09 (2.05) |
| 15 | 2.81 (1.50) |

## 4. Discussion

### 4.1 Effective modulus distributions

MC3T3 and MLO-A5 cells showed lower and less disperse effective moduli for both the nucleus and peripheral regions (Figure 3, Table 1). In contrast, the osteoblast-like and osteocyte-like IDG-SW3 cells showed wide dispersion ranges and higher values. This could be related to the intrinsic characteristics of the cell lines, given that they were acquired from different sources and were not differentiated from a single origin (Sugawara et al., 2008).

The distributions of effective moduli for the periphery were more dispersed than the ones for the nuclei. This was hypothesised to be linked to a less homogeneous structure of the cell outside the nucleus: while centring the measure over the nucleus provided consistency between cells, the peripheral measurements might have involved areas richer or poorer in specific intracellular components affecting the output stiffness. The periphery effective modulus showed higher values than the nuclear ones for all cell lines (Figure 3, Table 1). Similar trends were observed elsewhere for bone cells (Sugawara et al., 2008) and for other cell lines (e.g. epithelial cells (Berdyyeva et al., 2005; Sokolov et al., 2006), fibroblasts (Gavara and Chadwick, 2016), endothelial cells (Sato et al., 2000; Schaefer et al., 2014)). It has been proposed that peripheral regions stiffer than nuclear ones would be detected for cells with high levels of actomyosin (Gavara and Chadwick, 2016).

Most available stiffness measures for bone cells sit in the range of 0.5-15 kPa (Bacabac et al., 2008; Bongiorno et al., 2014; Docheva et al., 2008; Kelly et al., 2011; Muthukumaran et al., 2012; Sugawara et al., 2008; Takai et al., 2005; Titushkin and Cho, 2007; Yourek et al., 2014), in the range of those calculated in the present work. A more detailed comparison is made difficult by the employment of different cells, different contact models, different probe shapes (i.e. higher stiffness modulus values are obtained with sharp cantilevers with respect to beaded cantilevers (Chiou et al., 2013)) and loading rates (i.e. cells apparent stiffness modulus increases with the loading rate (Zhao et al., 2006)). Moreover, many studies report stiffness data as mean value and standard error of the mean. To this aim, multiple effective modulus values are first grouped (e.g. by cell or by location) and a mean value is calculated; then a variability range analysis is performed on these mean values to calculate their standard error. This representation does not allow for direct analysis of the population heterogeneity, as the dispersion is calculated on the mean values and not on the original data. Moreover, the average population modulus values are likely to be not normally distributed (i.e. the distribution is positively skewed as the stiffness cannot take negative values) and therefore the representation through a mean and not a median would result in calculating higher stiffness values unless some statistical corrections to render normality were applied.

## 4.2 Sample size analysis

We proposed a retrospective approach (Chen et al., 2016) to quantify the required sample size for AFM nanoindentation testing on cells. Large samples of four bone cell types and two separate regions (nucleus and periphery) were tested and analysed separately to build saturation curves for the coefficient of variation $CV_{\%}$ for increasing sample sizes. The value of effective modulus at convergence was calculated for each sample size by using a bootstrap resampling approach.

Despite the fact that the distributions of effective moduli were different for different cell lines and regions (Figure 3, Table 1), the calculated $CV_{\%}$ trend for increasing sample sizes was similar in all cases (Figure 5), suggesting a similar heterogeneity degree for all samples. This allowed fitting of the $CV_{\%}$ with a common curve of the form $y = ax^b$, which could be used to estimate *a priori* the sample size needed for future experiments with the same cell types.

The proposed fitting parameters are, in fact, specific for the present protocol and cell types and generalisation to different experimental setting or target cells should be avoided. A sensible approach would require using the present tool on a preliminary dataset in order to estimate the correct fitting parameters, following these steps:

1. Test a small number of cells (e.g. 10) of a given cell type and with a protocol of choice.
2. Post-process the data to obtain a stiffness measure for each cell.
3. Calculate the $CV_{\%}$ for increasing sample sizes (N = 1,2,…,10) with the presently proposed tool.

4. Fit a curve of the form $y = ax^b$ to the data to obtain the fitting parameters *a* and *b.*
5. Use the fitted curve to estimate the number of cells required to achieve a target maximum $CV_{\%}$ (e.g. 5% or 10%).

The analysis related to the optimisation of the required number of measurements per cell showed that averaging more measurements per cell gave less disperse effective modulus distributions (Figure 6, Table 2). The use of multiple measurements helped, in fact, smoothing out some heterogeneity likely ascribable to technical and not biological variation (Chen et al., 2016; Wagner et al., 2016). It should be noted that the median value calculated for the distributions using a different number of measurements per cell are different, highlighting the need for suitable data representation to fully capture the sample characteristics. The median value is in fact not sufficient and a distribution representation should be preferred.

Required sample sizes of 21 or 83 cells were computed for the employed cells and protocol if setting a threshold for a maximum $CV_{\%}$ of 10% or 5%, respectively. Despite the fact that AFM nanoindentation is not a high throughput technique being time- and user-intensive (Costa, 2004), these sample sizes are reasonable for an experienced user to acquire within a limited number of experiments. Moreover, they are much smaller than the ones suggested for other single-cell techniques, such as phenotyping, which can require minimum sample sizes of about 300 cells (Phillip et al., 2017).

### 4.3 Limitations of the present study and future directions

The Hertz model was used to calculate the elastic modulus from AFM force spectroscopy curves. This model was originally developed for a soft indenter on a rigid surface and the calculations were based on the assumption that the deformation of the sample was much smaller than the radius of the spherical probe (Hertz, 1881). This assumption does not apply when considering soft samples such as cells and therefore other fitting models have been proposed. A number of studies in the literature (e.g. Berdyyeva et al., 2005; Guz et al., 2014; Lekka et al., 1999) used the model derived by Sneddon for the case of a rigid indenter on a deformable surface (Sneddon, 1965) which does not hold constraints on the sample deformation and can be applied for indenters of different shapes. However, in the case of spherical indenters with a radius larger than approximately 1-2 μm, the Hertz model well approximates the Sneddon model despite its rigid assumptions and is more convenient for presenting an analytical form (Puricelli et al., 2015). Future improvements of the presented method should include analytical correction factors, to take into account the effect of the limited sample thickness and the contribution of the rigid substrate (Dimitriadis et al., 2002; Garcia and Garcia, 2018). This would allow for more precise determination of the effective modulus, particularly in the case of the cell periphery which displayed limited thickness.

Recently, a multicentre study aimed at standardising AFM procedures for soft biological samples suggested that the erroneous cantilever sensitivity determination was a major cause of discrepancies in the results between different labs, both for soft gels and cells (Schillers et al., 2017). A new standardised procedure was therefore proposed to calculate the correct deflection sensitivity from thermal fluctuations of the free cantilever with an independently determined value for the spring constant obtained with a vibrometer. This experimental error was however overlooked in the present work and therefore might have caused the results to not be fully repeatable. In future work, similar standardised methodologies should be incorporated as they would help to ascribe the correct degree of variability to cell physiological heterogeneity, further reducing the experimental inaccuracies. The sample size considerations discussed in the present work remain however valid and highlight the need for common procedures for AFM nanoindentation of biological samples.

All the measurements performed in the present work for cell mechanical properties focused on the cell stiffness represented by the effective modulus and therefore on the elastic

material characterisation. The viscoelastic characteristics of cells are however a key factor in the regulation of various cell processes (Abidine et al., 2013; Verdier, 2003). AFM has been used to characterise cell viscoelasticity by superimposing a low-amplitude sinusoidal oscillation on an initial cell indentation and by analysing the cell time-dependent response (Abidine et al., 2013; Alcaraz et al., 2003; Park et al., 2005; Raman et al., 2011). It could be of interest to evaluate the requirements for sample sizes if additional viscoelastic parameters would be taken into account.

The AFM nanoindentation data was limited to bone cells and the parameters obtained for the fitting curve of the sample size analysis should not be generalised to other cell types. It would be of interest, however, to test other cell types, both physiological and pathological, in order to verify how close the fitting parameters are to the present case. Given that the heterogeneity in terms of mechanical properties within a cell population is likely to be driven by similar biological phenomena (i.e. cell cycle, cell differentiation, migration, adhesion (Crisan and Dzierzak, 2016; Krieger and Simons, 2015; Satir, 2016; Wills et al., 2017)), it could be possible that global experimentally fitted parameters would work. This hypothesis requires however further verification and cannot be assumed valid *a priori*.

## 5. Conclusions

Single cell technologies represent a powerful tool to investigate cellular characteristics. However, the applicability of single cell analysis methods relies on the ability to measure enough entities so that the results are representative of a population or subpopulation of interest. For this reason, suitable power analyses should be performed in order to obtain reliable measurements of the metric of interest.

AFM nanoindentation experiments have been extensively used to test single cell mechanical properties in physiological and pathological conditions. However, the number of cells tested or the number of measurements per cell varied greatly between different studies and often were arbitrarily set. Hence, the present work proposes a tool to estimate the sample size required to obtained reliable measurements of stiffness for a cell population.

## 6. Acknowledgements

The work was supported by the EPSRC (“Multisim”, Grant No. EP/K03877X/1), the European Research Council (Grant No. 258321), and the University of Sheffield (“Mechanoreceptors in health and disease” Network Scholarship).

## References


Abidine, Y., Michel, R., Duperray, A., Verdier, C., 2013. Microrheology of complex systems and living cells using AFM. Comput. Methods Biomech. Biomed. Engin. 16, 15–16. https://doi.org/10.1080/10255842.2013.815961

Alcaraz, J., Buscemi, L., Grabulosa, M., Trepat, X., Fabry, B., Farré, R., Navajas, D., 2003. Microrheology of human lung epithelial cells measured by atomic force microscopy. Biophys. J. 84, 2071–9. https://doi.org/10.1016/S0006-3495(03)75014-0

Bacabac, R.G., Mizuno, D., Schmidt, C.F., MacKintosh, F.C., Van Loon, J.J.W. a, Klein-Nulend, J., Smit, T.H., 2008. Round versus flat: Bone cell morphology, elasticity, and mechanosensing. J. Biomech. 41, 1590–1598. https://doi.org/10.1016/j.jbiomech.2008.01.031

Berdyyeva, T.K., Woodworth, C.D., Sokolov, I., 2005. Human epithelial cells increase their rigidity with ageing in vitro : direct measurements. Phys. Med. Biol. 50, 81–92. https://doi.org/10.1088/0031-9155/50/1/007

Bongiorno, T., Kazlow, J., Mezencev, R., Griffiths, S., Olivares-Navarrete, R., McDonald, J.F., Schwartz, Z., Boyan, B.D., McDevitt, T.C., Sulchek, T., 2014. Mechanical stiffness as an improved single-cell indicator of osteoblastic human mesenchymal stem cell differentiation. J. Biomech. 47, 2197–2204. https://doi.org/10.1016/j.jbiomech.2013.11.017

Chen, X., Love, J.C., Navin, N.E., Pachter, L., Stubbington, M.J.T., Svensson, V., Sweedler, J. V., Teichmann, S.A., 2016. Single-cell analysis at the threshold. Nat. Biotechnol. 34, 1111–1118. https://doi.org/10.1038/nbt.3721

Chiou, Y.W., Lin, H.K., Tang, M.J., Lin, H.H., Yeh, M.L., 2013. The Influence of Physical and Physiological Cues on Atomic Force Microscopy-Based Cell Stiffness Assessment. PLoS One 8. https://doi.org/10.1371/journal.pone.0077384

Costa, K.D., 2004. Single-cell elastography: probing for disease with the atomic force microscope. Dis. Markers 19, 139–154. https://doi.org/10.1155/2004/482680

Crisan, M., Dzierzak, E., 2016. The many faces of hematopoietic stem cell heterogeneity. Development 143, 4571–4581. https://doi.org/10.1242/dev.114231

Dimitriadis, E.K., Horkay, F., Maresca, J., Kachar, B., Chadwick, R.S., 2002. Determination of Elastic Moduli of Thin Layers of Soft Material Using the Atomic Force Microscope. Biophys. J. 82, 2798–2810. https://doi.org/10.1016/S0006-3495(02)75620-8

Docheva, D., Padula, D., Popov, C., Mutschler, W., Clausen-Schaumann, H., Schieker, M., 2008. Researching into the cellular shape, volume and elasticity of mesenchymal stem cells, osteoblasts and osteosarcoma cells by atomic force microscopy: Stem Cells. J. Cell. Mol. Med. 12, 537–552. https://doi.org/10.1111/j.1582-4934.2007.00138.x

Garcia, P.D., Garcia, R., 2018. Determination of the Elastic Moduli of a Single Cell Cultured on a Rigid Support by Force Microscopy. Biophys. J. 114, 2923–2932. https://doi.org/10.1016/j.bpj.2018.05.012

Gavara, N., 2016. Combined strategies for optimal detection of the contact point in AFM force-indentation curves obtained on thin samples and adherent cells. Nat. Publ. Gr. 6:21267, 1–13. https://doi.org/10.1038/srep21267

Gavara, N., Chadwick, R.S., 2016. Relationship between cell stiffness and stress fiber amount, assessed by simultaneous atomic force microscopy and live-cell fluorescence imaging. Biomech. Model. Mechanobiol. 15, 511–523. https://doi.org/10.1007/s10237-015-0706-9

Guz, N., Dokukin, M., Kalaparthi, V., Sokolov, I., 2014. If Cell Mechanics Can Be Described by Elastic Modulus: Study of Different Models and Probes Used in Indentation

Experiments. Biophys. J. 107, 564–575. https://doi.org/10.1016/j.bpj.2014.06.033

Hertz, H., 1881. Über die Berührung faster elastischer Körper. J. die Reine Angew. Math. 156–171. https://doi.org/10.1515/crll.1882.92.156

Kato, Y., Boskey, a, Spevak, L., Dallas, M., Hori, M., Bonewald, L.F., 2001. Establishment of an osteoid preosteocyte-like cell MLO-A5 that spontaneously mineralizes in culture. J. Bone Miner. Res. 16, 1622–33. https://doi.org/10.1359/jbmr.2001.16.9.1622

Kelly, G.M., Kilpatrick, J.I., van Es, M.H., Weafer, P.P., Prendergast, P.J., Jarvis, S.P., 2011. Bone cell elasticity and morphology changes during the cell cycle. J. Biomech. 44, 1484–1490. https://doi.org/10.1016/j.jbiomech.2011.03.011

Kodama, H., Amagai, Y., Sudo, H., Kasai, S., Yamamoto, S., 1981. Establishment of a clonal osteogenic cell line from newborn mouse calvaria. J. Oral Biol. 23, 899–901. https://doi.org/10.2330/joralbiosci1965.23.899

Krieger, T., Simons, B.D., 2015. Dynamic stem cell heterogeneity. Development 142, 1396–1406. https://doi.org/10.1242/dev.101063

Krzywinski, M., Altman, N., 2013. Points of significance: Power and sample size. Nat. Methods 10, 1139–1140. https://doi.org/10.1038/nmeth.2738

Kuznetsova, T.G., Starodubtseva, M.N., Yegorenkov, N.I., Chizhik, S.A., Zhdanov, R.I., 2007. Atomic force microscopy probing of cell elasticity. Micron 38, 824–833. https://doi.org/10.1016/j.micron.2007.06.011

Lekka, M., 2016. Discrimination Between Normal and Cancerous Cells Using AFM. Bionanoscience 6, 65–80. https://doi.org/10.1007/s12668-016-0191-3

Lekka, M., Laidler, P., Gil, D., Lekki, J., Stachura, Z., Hrynkiewicz, a Z., 1999. Elasticity of normal and cancerous human bladder cells studied by scanning force microscopy. Eur. Biophys. J. 28, 312–316. https://doi.org/10.1007/s002490050213

Li, M., Liu, L., Xiao, X., Xi, N., Wang, Y., 2016. Viscoelastic Properties Measurement of Human Lymphocytes by Atomic Force Microscopy Based on Magnetic Beads Cell Isolation. IEEE Trans. Nanobioscience 15, 398–411. https://doi.org/10.1109/TNB.2016.2547639

Love, J.C., 2010. Integrated Process Design for Single-Cell Analytical Technologies. AIChE J. 56, 2496–2502. https://doi.org/10.1002/aic

Luo, Q., Kuang, D., Zhang, B., Song, G., 2016. Cell stiffness determined by atomic force microscopy and its correlation with cell motility. Biochim. Biophys. Acta - Gen. Subj. 1860, 1953–1960. https://doi.org/10.1016/j.bbagen.2016.06.010

Müller, D.J., Dufrêne, Y.F., 2011. Atomic force microscopy: A nanoscopic window on the cell surface. Trends Cell Biol. 21, 461–469. https://doi.org/10.1016/j.tcb.2011.04.008

Muthukumaran, P., Lim, C.T., Lee, T., 2012. Estradiol influences the mechanical properties of human fetal osteoblasts through cytoskeletal changes. Biochem. Biophys. Res. Commun. 423, 503–508. https://doi.org/10.1016/j.bbrc.2012.05.149

Navin, N.E., 2014. Cancer genomics: one cell at a time. Genome Biol. 15, 452. https://doi.org/10.1186/s13059-014-0452-9

Papalexi, E., Satija, R., 2017. Single-cell RNA sequencing to explore immune cell heterogeneity. Nat. Rev. Immunol. https://doi.org/10.1038/nri.2017.76

Park, S., Koch, D., Cardenas, R., Käs, J., Shih, C.K., 2005. Cell Motility and Local Viscoelasticity of Fibroblasts. Biophys. J. 89, 4330–4342. https://doi.org/10.1529/biophysj.104.053462

Pelkmans, L., 2012. Using Cell-to-Cell Variability— A New Era in Molecular Biology. Science

(80-. ). 336, 425–6. https://doi.org/10.1126/science.1222161

Phillip, J.M., Wu, P.H., Gilkes, D.M., Williams, W., McGovern, S., Daya, J., Chen, J., Aifuwa, I., Lee, J.S.H., Fan, R., Walston, J., Wirtz, D., 2017. Biophysical and biomolecular determination of cellular age in humans. Nat. Biomed. Eng. 1. https://doi.org/10.1038/s41551-017-0093

Puricelli, L., Galluzzi, M., Schulte, C., Podestà, A., Milani, P., 2015. Nanomechanical and topographical imaging of living cells by atomic force microscopy with colloidal probes. Rev. Sci. Instrum. 86. https://doi.org/10.1063/1.4915896

Raman, A., Trigueros, S., Cartagena, A., Stevenson, A.P.Z., Susilo, M., Nauman, E., Contera, S.A., 2011. Mapping nanomechanical properties of live cells using multi-harmonic atomic force microscopy. Nat. Nanotechnol. 6, 809–814. https://doi.org/10.1038/nnano.2011.186

Satir, P., 2016. Chirality of the cytoskeleton in the origins of cellular asymmetry. Philos. Trans. R. Soc. B Biol. Sci. 371. https://doi.org/10.1098/rstb.2015.0408

Sato, M., Nagayama, K., Kataoka, N., Sasaki, M., Hane, K., 2000. Local mechanical properties measured by atomic force microscopy for cultured bovine endothelial cells exposed to shear stress. J. Biomech. 33, 127–135. https://doi.org/10.1016/S0021-9290(99)00178-5

Schaefer, A., te Riet, J., Ritz, K., Hoogenboezem, M., Anthony, E.C., Mul, F.P.J., de Vries, C.J., Daemen, M.J., Figdor, C.G., van Buul, J.D., Hordijk, P.L., 2014. Actin-binding proteins differentially regulate endothelial cell stiffness, ICAM-1 function and neutrophil transmigration. J. Cell Sci. 127, 4470–4482. https://doi.org/10.1242/jcs.154708

Schillers, H., Rianna, C., Schäpe, J., Luque, T., Doschke, H., Wälte, M., Uriarte, J.J., Campillo, N., Michanetzis, G.P.A., Bobrowska, J., Dumitru, A., Herruzo, E.T., Bovio, S., Parot, P., Galluzzi, M., Podestà, A., Puricelli, L., Scheuring, S., Missirlis, Y., Garcia, R., Odorico, M., Teulon, J.M., Lafont, F., Lekka, M., Rico, F., Rigato, A., Pellequer, J.L., Oberleithner, H., Navajas, D., Radmacher, M., 2017. Standardized Nanomechanical Atomic Force Microscopy Procedure (SNAP) for Measuring Soft and Biological Samples. Sci. Rep. 7, 1–9. https://doi.org/10.1038/s41598-017-05383-0

Sneddon, I.N., 1965. The relation between load and penetration in the axisymmetric Boussinesq problem for a punch of arbitrary profile. Int. J. Eng. Sci. 3, 47–57. https://doi.org/10.1016/0020-7225(65)90019-4

Sokolov, I., Iyer, S., Woodworth, C.D., 2006. Recovery of elasticity of aged human epithelial cells in vitro. Nanomedicine Nanotechnology, Biol. Med. 2, 31–36. https://doi.org/10.1016/j.nano.2005.12.002

Sugawara, Y., Ando, R., Kamioka, H., Ishihara, Y., Murshid, S. a., Hashimoto, K., Kataoka, N., Tsujioka, K., Kajiya, F., Yamashiro, T., Takano-Yamamoto, T., 2008. The alteration of a mechanical property of bone cells during the process of changing from osteoblasts to osteocytes. Bone 43, 19–24. https://doi.org/10.1016/j.bone.2008.02.020

Takai, E., Costa, K.D., Shaheen, A., Hung, C.T., Guo, X.E., 2005. Osteoblast elastic modulus measured by atomic force microscopy is substrate dependent. Ann. Biomed. Eng. 33, 963–971. https://doi.org/10.1007/s10439-005-3555-3

Titushkin, I., Cho, M., 2007. Modulation of cellular mechanics during osteogenic differentiation of human mesenchymal stem cells. Biophys. J. 93, 3693–702. https://doi.org/10.1529/biophysj.107.107797

Tsioris, K., Torres, A.J., Douce, T.B., Love, J.C., 2014. A New Toolbox for Assessing Single Cells. Annu. Rev. Chem. Biomol. Eng. 5, 455–477. https://doi.org/10.1146/annurev-chembioeng-060713-035958

Verdier, C., 2003. Rheological properties of living materials. From cells to tissues. J. Theor. Med. 5, 67–91. https://doi.org/10.1080/10273360410001678083

Wagner, A., Regev, A., Yosef, N., 2016. Revealing the vectors of cellular identity with single-cell genomics. Nat. Biotechnol. 34, 1145–1160. https://doi.org/10.1038/nbt.3711

Wang, L., Livak, K.J., Wu, C.J., 2017. High-dimension single-cell analysis applied to cancer. Mol. Aspects Med. https://doi.org/10.1016/j.mam.2017.08.005

Wills, Q.F., Mellado-Gomez, E., Nolan, R., Warner, D., Sharma, E., Broxholme, J., Wright, B., Lockstone, H., James, W., Lynch, M., Gonzales, M., West, J., Leyrat, A., Padilla-Parra, S., Filippi, S., Holmes, C., Moore, M.D., Bowden, R., 2017. The nature and nurture of cell heterogeneity: accounting for macrophage gene-environment interactions with single-cell RNA-Seq. BMC Genomics 18, 53. https://doi.org/10.1186/s12864-016-3445-0

Wittkowske, C., Reilly, G.C., Lacroix, D., Perrault, C.M., 2016. In Vitro Bone Cell Models: Impact of Fluid Shear Stress on Bone Formation. Front. Bioeng. Biotechnol. 4. https://doi.org/10.3389/fbioe.2016.00087

Woo, S.M., Rosser, J., Dusevich, V., Kalajzic, I., Bonewald, L.F., 2011. Cell line IDG-SW3 replicates osteoblast-to-late-osteocyte differentiation in vitro and accelerates bone formation in vivo. J. Bone Miner. Res. 26, 2634–2646. https://doi.org/10.1002/jbmr.465

Yourek, G., Hussain, M.A., Mao, J.J., 2014. Cytoskeletal changes of mesenchymal stem cells during differentiation. ASAIO J. 53, 219–28. https://doi.org/10.1097/MAT.0b013e31802deb2d

Zhao, M., Srinivasan, C., Burgess, D.J., Huey, B.D., 2006. Rate- and depth-dependent nanomechanical behavior of individual living Chinese hamster ovary cells probed by atomic force microscopy. J. Mater. Res. 21, 1906–1912. https://doi.org/10.1557/jmr.2006.0233